Residual stress distribution in steel butt welds measured using neutron and synchrotron diffraction

2009 J. Phys.: Condens. Matter 21 124213

(http://iopscience.iop.org/0953-8984/21/12/124213)

J. Phys.: Condens. Matter **21** (2009) 124213 (8pp) doi:10.1088/0953-8984/21/12/124213

Residual stress distribution in steel butt welds measured using neutron and synchrotron diffraction

A M Paradowska[1], J W H Price[2], T R Finlayson[3], U Lienert[4], P Walls[5] and R Ibrahim[2]

[1] ISIS Facility, Science and Technology Facility Council, Rutherford Appleton Laboratory, Didcot OX11 0QX, UK
[2] Department of Mechanical Engineering, Monash University, Victoria 3800, Australia
[3] School of Physics, University of Melbourne, Victoria 3010, Australia
[4] Advanced Photon Source, Argonne National Laboratory, 9700 South Cass Avenue, Argonne, IL 60439, USA
[5] Institute of Materials and Engineering Science, ANSTO, Lucas Heights, NSW 2234, Australia

E-mail: anna.paradowska@stfc.ac.uk

Received 27 October 2008, in final form 19 December 2008
Published 25 February 2009
Online at stacks.iop.org/JPhysCM/21/124213

Abstract
70 keV synchrotron radiation and thermal neutrons have been employed to investigate the residual stress characteristics in a fully restrained, steel, butt weld. The focus is on the values of the subsurface and through-thickness strain/stress variation in the middle of the weld. The advantages and limitations of the techniques have been addressed, in relation to the gauge volume, the stress-free reference sample and positioning. The measurement of residual stress around the weld achieved in this work significantly improves the resolution at which residual stress in welded components has been determined.

(Some figures in this article are in colour only in the electronic version)

1. Introduction

In welded structures residual stresses are formed primarily as the result of differential contractions which occur as the weld metal solidifies and cools to ambient temperature. The temperature distribution in the weldment is not uniform and changes as the welding progresses. The temperature and temperature distributions affect expansion and contraction and the relationship between stress and strain and thus, residual stresses (RS) [1]. RS have a significant effect on corrosion, fracture resistance, creep and corrosion/fatigue performance and a full understanding of these stresses is desirable. Therefore, experimental measurements are essential to establish a quantitative understanding of the sign, magnitude and distribution of the RS around the repair, within acceptable limits. RS in welded joints and repairs are sometimes reduced by post-weld heat treatment (PWHT) [2] or by mechanical stress relieving [3]. RS are considered in fitness-for-purpose assessments such as BS 7910 [4] and R6 [5], although only simple conservative models are used for the residual stress distribution.

Theoretical and numerical research has been carried out in recent years to study the effect of RS on weld repairs [1, 6]. However, quantitative theoretical analysis of RS in repair weldments using modelling techniques such as the non-linear, finite-element method (FEM) is not, at present, a practical engineering design tool due to the complexity of the analysis [7]. The analysis is non-linear in at least three ways: the variation in material properties over the large temperature range involved; the material deformation and phase transformation characteristics; the heat-transfer characteristics of the welding.

Many non-destructive and destructive techniques are employed for detecting RS in welded components [8], such as hole drilling, conventional x-ray, neutron (ND), synchrotron diffraction (SD) or ultrasonic examination. No technique can measure the residual strain at a single point in a component, but rather every technique measures a strain integrated in

Table 1. Chemical compositions of the parent and weld metals (in wt%).

	C	Mn	Si	S	P	Ni	Cr	Mo	Cu	V	Ti	Co	Al
Parent metal	0.15	1.35	0.28	0.01	0.02	0.02	0.01	0.01	0.01	<0.01	<0.01	<0.01	0.03
Weld metal	0.10	1.7	0.68	0.02	0.02	0.05	0.03	0.04	—	0.04	—	—	—

some way over a sampled gauge volume. The gauge volume thus corresponds approximately to the spatial resolution of the measurements. In many cases, much can be learnt from the complementary use of more than one technique. In particular, for steel, each application of these techniques has its limitations in terms of the effective penetration depth.

Non-destructive measurement is a key issue in the confirmation of the theoretical work. ND and SD are outstanding in their ability to obtain RS non-destructively within the subsurface and interior of components [9, 10]. Neutrons can evaluate the weld structure in three directions, with spatial resolution of 1 mm (or less) to a depth of many millimetres below the weld surface (up to 50 mm for steel). An international standard ISO/TS 21432-2005 [11] for measuring RS using ND is being developed on a ring-plug fit to achieve reproducible and reliable stress measurements.

The use of synchrotron radiation for residual stress-measurement permits two-dimensional measurements are possible with very useful beam penetration [12]. The penetration is achieved with high-energy (short-wavelength) radiation that gives Bragg diffraction at small angles. Under these circumstances the gauge volume is needle-like resulting in a small number of grains in the gauge volume. This technique was successfully applied to estimate RS in aluminium welds [13, 14] and to measure the strains in welded components [15–17]. For all diffraction techniques, the estimate of the absolute value of the strain being measured relies on the use of a zero-stress, reference sample. Thus there is a requirement for the preparation of a zero-stress, reference sample from a companion weld or destructively from the weld itself after the measurements.

In work reported in this paper, synchrotron diffraction at the Advance Photon Source (APS), Chicago, USA and neutron diffraction at The Australian Nuclear Science and Technology Organization (ANSTO), Lucas Heights, Australia were used to establish detailed residual strain/stress distributions in welded components. The advantages and limitations of strain scanning using both techniques, with the application to welded components, are discussed. The experimental results from ND and SD data will be compared to evaluate the RS in weldments.

2. Experimental details

2.1. Materials and welding procedure

The material used in this study was a carbon steel. The chemical compositions of the parent and weld metals are shown in table 1. The dimensions of the plates for a 'V' butt weld were 300 × 150 × 12 mm^3. Two samples were manufactured, one being used for residual stress measurements and the other for destructive testing and reference sample preparation. A schematic outline of the experimental procedure is shown in figure 1. Each sample was a butt weld with a 60° preparation angle and a 2 mm gap between the plates (figure 1(a)). Four beads were deposited to fill the weld, produced using flux-cored, arc welding (FCAW) with an E71T-5 consumable and an Ar77%/$CO_2$23% shielding gas. The specimen was mounted under an automatic-speed-controlled, welding torch. The welding parameters are shown in table 2. The samples were fully restrained during the welding process by several tack welds which where removed after sample cool-down to ambient temperature.

Table 2. Welding parameters used in the experimental work.

Parameter	Run (1)	Runs (2–4)
Electrode diameter (mm)	1.6	1.6
Current range (A)	260–280	260–280
Voltage range (V)	28–30	28–30
Traverse speed (mm min^{-1})	480	360
Wire-feeding speed (mm min^{-1})	3600	3600
Electrode stick-out distance (mm)	20	20
Gas flow rate (min^{-1})	20	20

2.2. Thermal cycle history

The main purpose of this part of the experiment was to record the temperatures in the heat affected zone (HAZ) and the parent metal (PM) during welding, as well as the cooling rate after the welding process was completed. The thermal histories were measured on the welding rig at ANSTO, using the NeoThermo TVS-600 Series thermal video camera. This apparatus can visualize surface temperatures with an appropriate chromatic scale. Temperature was logged in four-second intervals by the digital thermographic camera during both the welding and cooling phases. The emissivity of the surface has been made uniform and equal to 0.97 by painting the parent metal black. A DataTaker DT3 logging up to 8 Type K thermocouples and the DataTaker software were used to record welding and cooling rates.

The thermal histories were measured during welding using the infrared camera and validated by five thermocouples (TC) which were attached to the surface of the sample. The thermocouples were placed in holes (1 mm in diameter and 1.5 mm in depth) in the middle of the sample at 5, 10, 15, 25 and 40 mm, respectively, from the edge of the 'V' preparation. A typical image obtained from the infrared camera and analysed using 'Thermalmonitor' software after the 4th bead was deposited is shown in figure 2, and the thermal histories, as recorded by the TC, are shown in figure 3. The streamlined contours (figure 2) had visually indicated that, after the 4th bead was deposited on the opposite side of the weld, the symmetrical heating was shifted towards the last-deposited bead. The dashed red line in figure 3 corresponds to

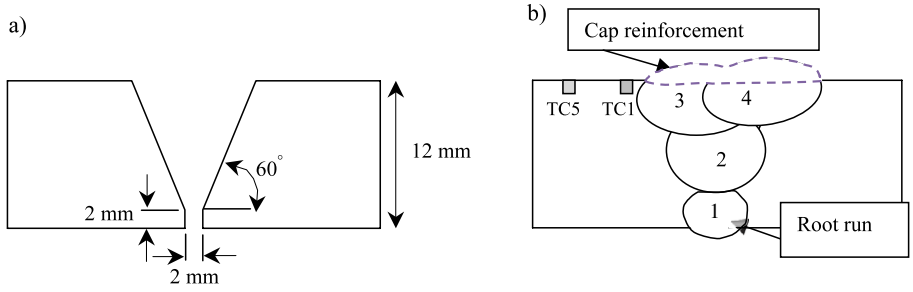

Figure 1. Schematic illustration of the experimental procedure showing (a) preparation of the plate and (b) the sequence of weld passes and positions of the thermocouples.

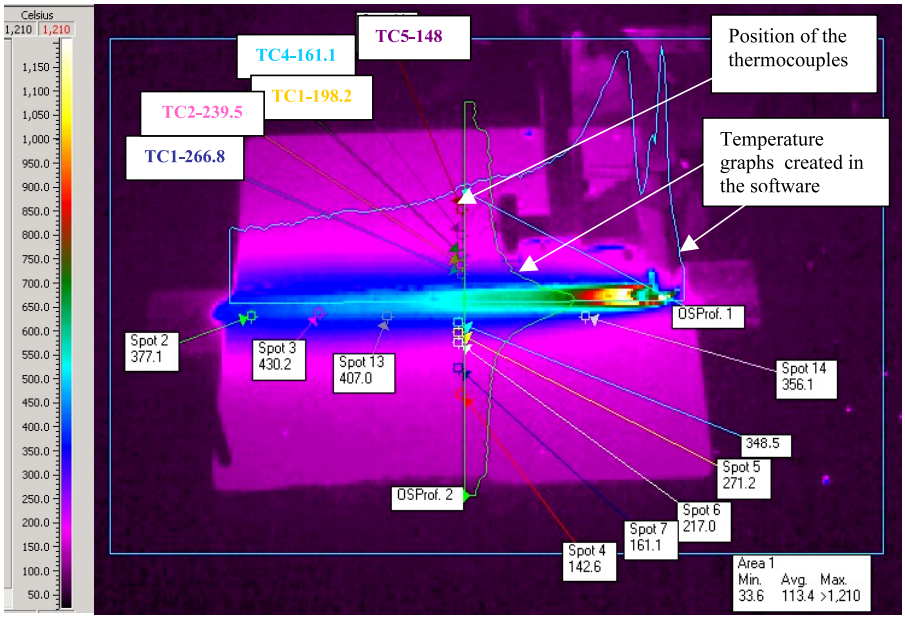

Figure 2. Thermal distribution across the butt weld after deposition of the 4th bead (after 1476 s of recording), using the infrared camera and calculated from the 'Thermalmonitor' software at various positions as indicated by the 'Spot' boxes.

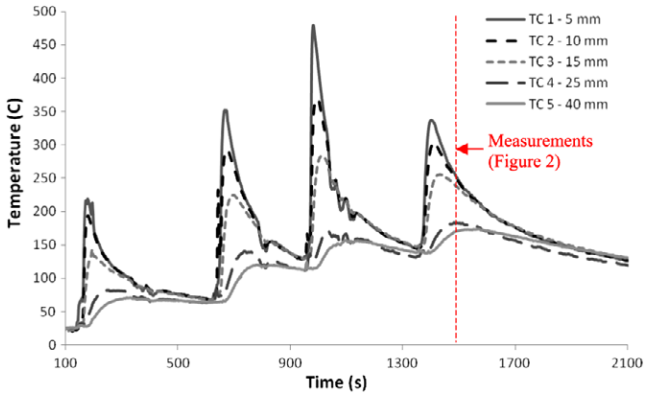

Figure 3. Temperature history of the butt weld, recorded by the thermocouples (TC).

the temperature profile indicated by the readings from the TC in figure 2 (at 1476 s from the start of recording the welding process).

The numbers in the boxes in figure 2 represent the temperatures calculated by the software. These data were collected to prove consistency in the welding procedure. The streamlined contour visually indicates that symmetrical heating was attained on both sides of the centre line of the weld. Temperature readings between the thermocouple and infrared thermography show good agreement and are within ±20 °C. Since the flame and other effects interfere with measurements around the weld pool, adequate measurements in the molten zone are not possible. However, the thermographic technique proved to be a useful tool in studying the heating of the sample outside the weld pool, as well as the cooling behaviour of the welds. Therefore this technique has the potential to measure and evaluate the post-weld-cooling behaviour of welded components.

2.3. Macroscopic inspection and hardness

Transverse sections were taken across all samples for macroscopic inspection and an example is shown in figure 4.

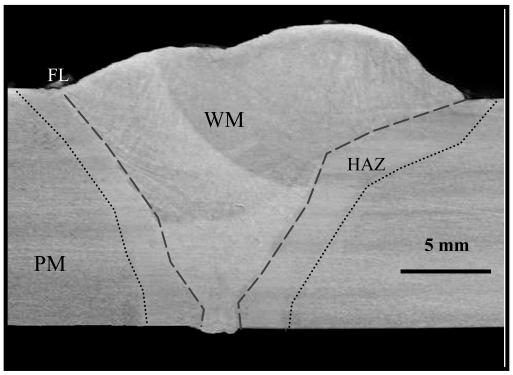

Figure 4. Micrograph of the transverse cross-section of a butt weld, showing the weld metal (WM), fusion line (FL), heat affected zone (HAZ) and parent metal (PM).

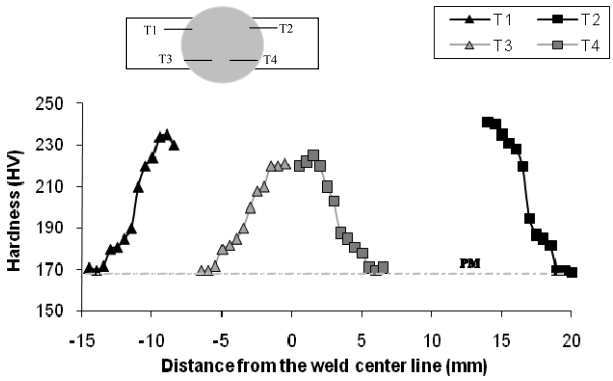

Figure 5. Vickers hardness measurements on the cross-section of a butt weld. The top-left inset illustrates the positions of the hardness profiles in the weld cross-section.

Hardness profiles were measured using a 5 kg indentation load on a cross-section of the weldment. Measurements were taken along a line 1.5 mm inside the original top and bottom plate surfaces, as illustrated in an inset to figure 5 in which the hardness data are presented. This information was obtained to establish the change in the hardness across the weld, HAZ and parent metal.

3. Residual stress evaluation

3.1. Neutron diffraction measurements

ND measurements of RS were undertaken on The Australian Strain Scanner (TASS) at ANSTO, Australia. The neutron wavelength used was 1.40 Å. Measurements were made using the αFe(211) reflection, at the detector angle, 2θ, of approximately 73.5° and the scattering vector parallel to each of the three axes identified as longitudinal (parallel to the length of the weld), transverse (perpendicular to the length of the weld and parallel to the plate) and normal (perpendicular to the length of the weld and perpendicular to the plate). The gauge volume is formed by 'slits' of a neutron absorbing material (cadmium) in the incident and diffracted beams. (See figure 6.) For the longitudinal measurements this gauge volume was approximately 1.5 × 1.5 × 2 mm^3 but for the transverse and normal measurements this gauge volume could be relaxed in one direction to 1 × 1 × 20 mm^3. This was possible on account of the lack of spatial variation for the transverse and normal components along the length of the weld and at its centre, allowing an increased neutron intensity (with consequent reduction in counting times) for each of these two measurements. In all cases, the sample was positioned so that the centre of the gauge volume was 1.5 mm below to top surface of the original PM. The experimental details for the ND measurements are summarized in table 3.

To establish the 'stress-free' lattice parameter, d_0, a 'comb' reference sample was produced by electro-discharge machining. (For more details see [18].) The 'comb' was cut from an identical weldment in the middle of the weld. The d_0 measurements were made using the same instrument settings as for the longitudinal strain measurements (table 3). The 'comb'

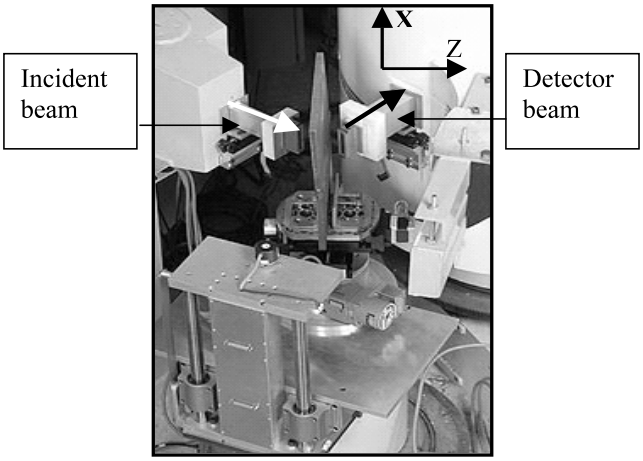

Figure 6. Overview of the Australian strain scanner (TASS) at HIFAR at ANSTO, Australia, showing a weldment sample mounted in position. In this orientation, the scattering vector is approximately parallel to the weld, as for the collection of the longitudinal strain component data.

had a tooth size of 3 × 3 × 6 mm^3 in one row of 19 teeth on the side of the reinforcement cap (figure 1) and 10 teeth of 3 × 3 × 5 mm^3 on the root side. Collected data indicated that for these particular alloys and welds, there are no significant effects on the d_0 in the welded region due to inhomogeneous microstructure or chemical composition changes. Therefore the average of all measurements across the 'comb' reference sample was used to determine the strains at all the points in the weldment. Residual strain values were then calculated from the d-spacing measurements for the αFe(211) Bragg reflection and this average d_0.

The longitudinal, transverse and normal components of the residual stress field were calculated for each strain-measurement position in the weldment from the relevant three strain components, using standard elasticity theory and assuming an elastically isotropic material and that the measurement directions correspond to the principal axes of the stress tensor [19]. For this conversion a Young's modulus of 207 GPa and Poisson's ratio of 0.3 were used.

Table 3. Comparison of experimental details for SD and ND measurements.

Diffraction parameter	Synchrotron x-rays (APS)	Neutron (TASS (ANSTO))
RS measurements dimensions	2D	3D
αFe(211) scattering angle ($2\theta_{211}$)	7.90°	73.40°
Incident beam size	20×20 μm^2	1×20 mm^2 (transverse and normal), 1.5×2 mm^2 (longitudinal)
Gauge volume	$20 \times 20 \times 114$ μm^3 (transverse and longitudinal)	$1 \times 1 \times 20$ mm^3 (transverse and normal), $1.5 \times 1.5 \times 2$ mm^3 (longitudinal)
Time for measurements	60 s (transverse and longitudinal)	20 min (transverse and normal), 60 min (longitudinal)
Precision	$\pm 10 \times 10^{-6}$ strain	$\pm 60 \times 10^{-6}$ strain
Reference d_0	'Comb'	'Comb'
Gauge volume for d_0	$20 \times 20 \times 200$ μm^3 (transverse and longitudinal)	$1.5 \times 1.5 \times 2$ mm^3 (transverse and longitudinal)

3.2. Synchrotron diffraction measurements

SD measurements were performed at the 1-ID beamline of the Advance Photon Source (APS), at Argonne National Laboratory, Chicago, USA. Monochromatic, 70 keV x-rays were used in transmission geometry and complete diffraction rings were recorded on an area detector (general electric amorphous silicon detector) as shown in figure 7. The presence of strains within the sample results in an azimuth-dependent, radial deformation of the diffraction rings. The measurement directions are given by the scattering vectors which for a given *hkl* reflection make an angle of 90°-θ_{hkl} to the incident beam, where θ_{hkl} is the *hkl* Bragg angle. Bragg angles are typically only a few degrees for high-energy x-rays and the diffraction-ring distortion measures, to good approximation, strains perpendicular to the incident beam. Thus, for the weldment in the position shown in figure 7, the radial diffraction-ring deformations in the horizontal and vertical directions measure the longitudinal and transverse strains, respectively. The experimental details in comparison to those for ND are shown in table 3.

To achieve spatial resolution along the beam, a conical slit cell was positioned behind the sample (figure 7). It defines the gauge length through the thickness of the sample, by the principle of crossed beams. Because of the small scattering angles this through-thickness gauge length is typically five to ten times larger than those perpendicular to the incident beam which were 20 μm, as defined by the incident beam slits [20]. For the weldment oriented as in figure 7, there would be negligible spatial variation along the length of the weld, near its centre.

Thus, is was reasonable to achieve grain averaging to enhance the diffraction-ring homogeneity, by translating the sample horizontally (perpendicular to the incident beam) during detector exposures (see figure 7). The same stress-free, reference sample was used and the same procedure applied to determine the spatial dependence of the transverse and longitudinal residual strain components as for the ND measurements.

The specimen geometry, coupled with x-ray absorption, precludes the measurement of the normal strain component. Thus to convert the measured strains to stress components, the additional assumption is made that the normal stress component is zero.

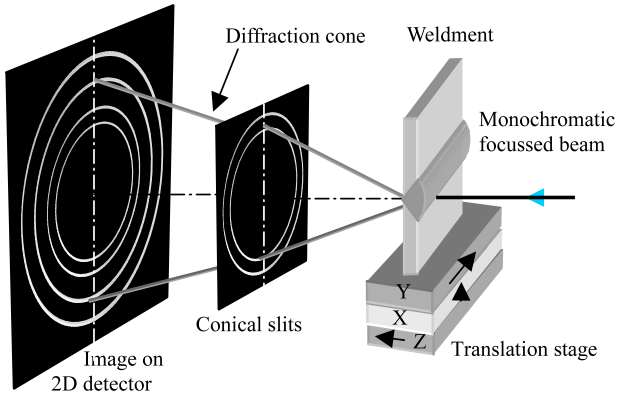

Figure 7. Schematic showing the low-angle, transmission, experimental set-up for SD at the APS.

4. Results and discussion

The residual microstrains measured from ND and SD are plotted in figure 8(a). The error bars, based on the uncertainties in the measured peak diffraction angles, were usually smaller than 20 microstrain for SD and 50–70 microstrain for ND. The measurements were taken every 1 mm across the sample using SD, as the sampling of the area is very fast (table 3). ND is a much more time consuming experiment. Therefore data points were closely spaced in the WM, but in larger steps in the HAZ and PM. Plots of relative peak intensity and relative full width at half maximum (FWHM) for the SD data are shown in figures 8 (b) and (c), respectively. Correlation with the intensity allows a confirmation of the position of the gauge volume in the weldment, with the intensity minimum at the centre of the last-deposited bead and with the toes easily visible at $x = \pm 10$ mm. The FWHM distribution shows a high plastic deformation in the weld, with a decrease in the HAZ.

Good agreement was found between the ND and SD data for the variation of microstrain with distance. Some small differences in the WM region where local variation with position are to be expected on account of the multi-bead welding, may be explained by the difference in the scattering gauge volumes for the two techniques (a through-thickness, needle-like volume for SD and a small prism for ND). In

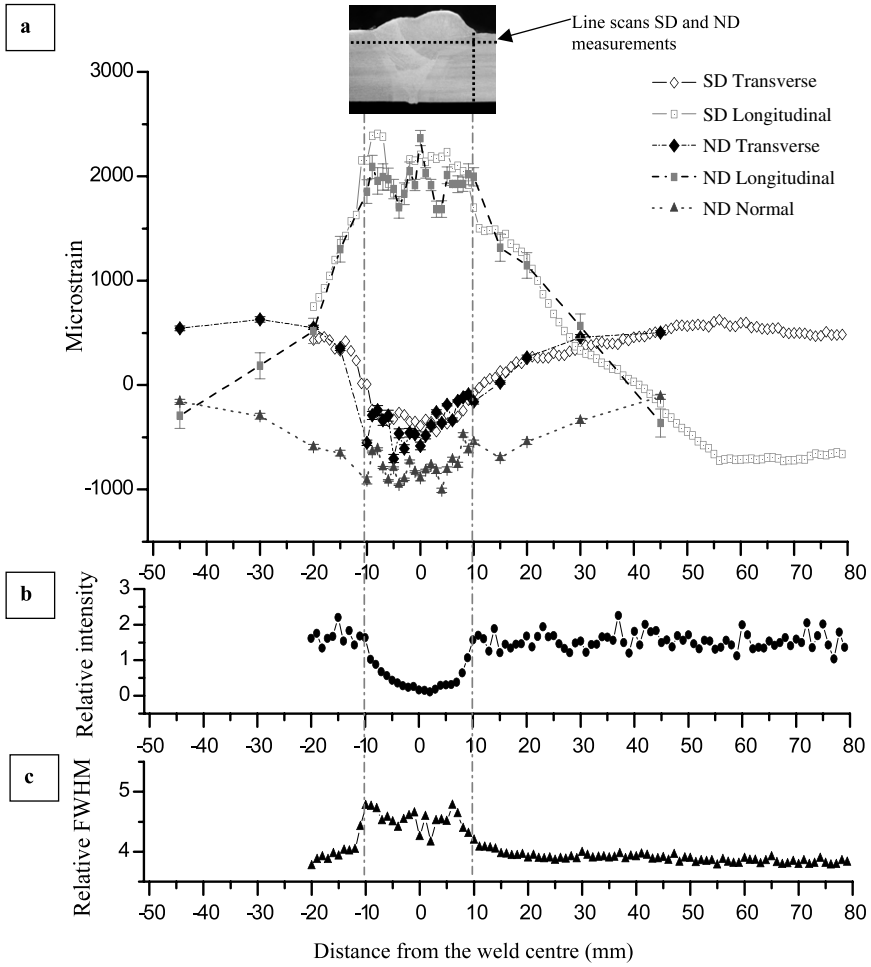

Figure 8. (a) Comparison of residual microstrain measured (at 1.5 mm below the surface of the PM plates) by synchrotron diffraction (SD) and neutron diffraction (ND); (b) Relative intensity and (c) relative full width at half maximum (FWHM) calculated from SD data. Note that the error bars for the SD measurements are smaller than the size of the data points (on average 20 microstrain in the PM and 30 microstrain in the HAZ and WM).

the SD data, for which the number of data points was larger, a distinct shoulder was observed in the longitudinal residual strain component in the HAZ about 12 mm from the weld centre, particularly on the side of the last-deposited bead. A similar shoulder for measurements in a ferritic steel weld has been observed previously and attributed to effects of the bainitic phase transformation in the steel [21].

The variations in the residual stress components are plotted in figure 9. In particular, for the components determined by ND, the longitudinal component is very high and tensile in the region of the WM and at the weld toe, up to the yield strength of the weld material. The errors shown on the data points are a consequence of the errors calculated for the strain components and are less than 7% of the yield stress of the PM. The transverse components are lower, up to 110 MPa at the toe on the side of the last-deposited bead, and to −60 MPa on the opposite side. The values of the RS are also high in the PM, up to 150 MPa at ±30 mm from the weld centre. This may be due to the larger size of the weldment, which results in a higher constraint condition.

The longitudinal and transverse RS measured by SD follow the same trends as those for ND. Differences are to be expected not only on account of the necessary assumption of a zero normal component but also on account of the distinctly different gauge volumes.

Figure 10 shows a comparison of through-thickness residual strains and stresses at the toe of the weld measured by SD and ND. These data were taken on the side where the last bead was deposited. From the ND data it was found that the normal residual stress component did not vary significantly through the thickness and the value is very close to zero. Thus the necessary assumption of zero for the normal stress component in converting strains to stresses in the case of the SD data, is now quite reasonable, allowing a direct comparison of the ND and SD determined stresses, as in figure 10. High, tensile, longitudinal strains and stresses were found through the thickness of the weld (between 350 and 400 MPa). Compressive transverse residual strain (stress) was found at the toe, which changed to low tension strain (stress) at a depth of 2 mm. The maximum value of the transverse residual stress component was found around the middle of the thickness of the plate, with readings of 175 MPa from the SD data and 215 MPa from ND data.

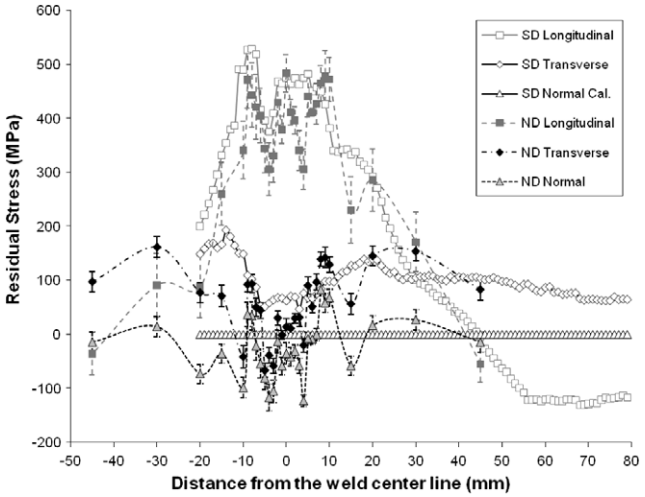

Figure 9. Residual stress distributions across the butt weld, measured by neutron and synchrotron diffraction (1.5 mm below the surface of the parent metal). Normal residual stress by SD is a direct result of the assumption that the normal stress component being equal to zero is used for the stress calculations. Note that the error bars for the SD measurements are smaller than the size of the data points (on average 7 MPa in the PM and 10 MPa in the HAZ and WM).

5. Conclusions

During the multi-pass, fusion welding, the HAZ of the PM experienced quite severe thermal cycles of rapid heating and cooling, which can be clearly seen from the thermal cycle history, and was confirmed by the microstructural changes and high hardness, in particular at the weld toes, where the last-solidified beads were deposited. High longitudinal RS were found within the weld as well as at the weld toe, reaching, or even exceeding, the uniaxial yield value. Additionally, in the region of the HAZ the longitudinal residual stress varied rapidly from highly tensile in the weld to a balancing compressive value in the PM.

Transverse residual stresses are much smaller, however they are tensile and that may be detrimental to the weldment as in many cases in-service stresses will usually superimpose on that direction. Quantitative reliable measurements with high spatial resolution are vital for the welding industry.

Neutron and synchrotron diffraction methods, for evaluation of RS in the WM, HAZ and PM have been explored. Owing to differences in beam penetration, scattering angles and beam sizes, the diffraction techniques are complementary to each other, rather than competitive. It is shown that it is possible to achieve good agreement in the spatial distributions and magnitudes for measurements from each of the techniques, provided the necessary assumption of a zero normal stress component is reasonable. But only ND can provide the full set of stress components.

To fully understand and estimate the residual strains/stresses in welds, the authors have recently shown how to use the thermal history and measured residual strain/stress profiles coupled with finite-element modelling to benchmark a bead-on-plate welding geometry [22]. Such work will be extended to more complex welding configurations such as the multi-pass, butt weld described here.

Acknowledgments

This work was conducted with the assistance of an Australian Research Council grant supported by the Welding Technology

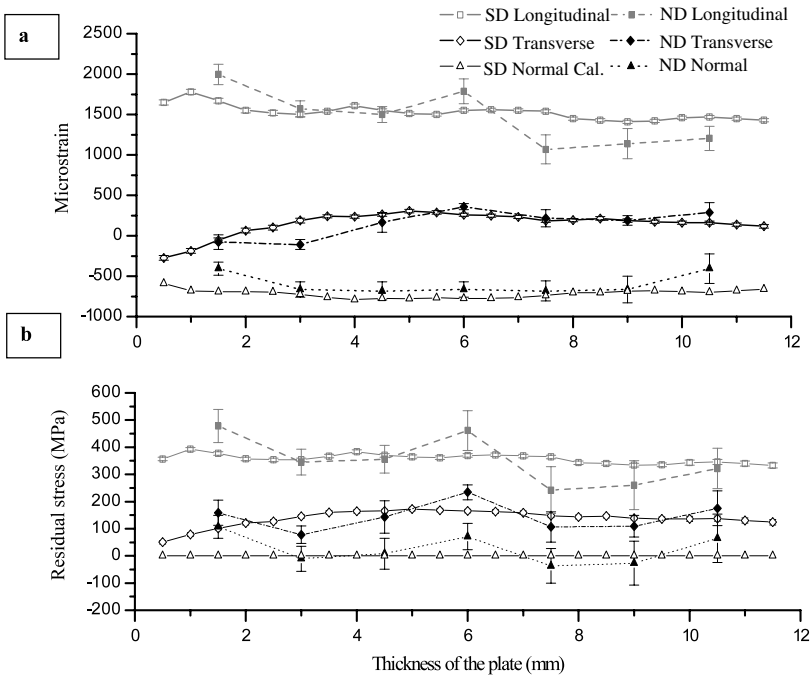

Figure 10. Comparison of (a) residual microstrain and (b) stress at the weld toe through the thickness of the butt weld, measured by synchrotron and neutron diffraction.

Institute of Australia (WTIA). Other assistance has been received from the Monash University Research Fund and the Australian Nuclear Science and Technology Organization (ANSTO). The Australian Institute of Nuclear Science and Engineering (AINSE) is acknowledged for financial assistance (Award No. AINSTU1604) to enable measurements on TASS to be conducted. The authors also thank the Australian Synchrotron Research Programme (ASRP) (Award No. SRI-127) enabling measurements on the 1-ID beamline at the Advance Photon Source (APS), to be carried out. Use of the APS was supported by the US Department of Energy, Office of Science, Office of Basic Energy Sciences, under Contract No. W-31-109-ENG-38.

References

[1] Myers P S, Uyeheara O A and Borman G L 1967 Fundamentals of heat flow in welding *Weld. Res. Council Bull.* 5
[2] Sedek P, Brozda J, Wang L and Withers P J 2003 *Int. J. Press. Vessels Pip.* **80** 705
[3] Yang Y S and Lee S H 1997 *Int. J. Press. Vessels Pip.* **73** 175
[4] BS 7910 1999 *Guide on Methods for Assessing the Acceptability of Flaws in Metallic Structures* (London: BSI, British Standards)
[5] Milne I, Ainsworth R A, Dowling A R and Stewart A T 2001 Assesment of the integrity of structures containing defects *CEGB Report R/H/R6-Rev. 4*
[6] Gandy D W, Finland S J and Viswanathan R 2001 *Trans. ASME* J **123** 157
[7] Dong P 2000 *Trans. ASME* J **123** 207
[8] Withers P J and Bhadeshia H K 2001 *Mater. Sci. Technol.* **17** 355
[9] Owen R A, Preston R V, Withers P J, Shercliff H R and Webster P J 2003 *Mater. Sci. Eng.* A **346** 159
[10] Webster G A and Wimpory R C 2001 *J. Neutron Res.* **9** 281
[11] iSO/TTA 3 2001 *Polycrystalline Materials—Determination of Residual Stresses by Neutron Diffraction*
[12] Withers P J 2003 Use of synchrotron x-ray radiation for stress measurements *Analysis of Residual Stress by Diffraction Using Neutron and Synchrotron Radiation* ed M E Fitzpatrick and A Lodini (London: Taylor and Francis) p 170
[13] Steuwer A, Peel M and Withers P J 2006 *Mater. Sci. Eng.* A **441** 187
[14] Peel M, Steuwer A, Preuss M and Withers P J 2003 *Acta Mater.* **51** 4791
[15] Paradowska A M, Price J W H, Finlayson T R, Lienert U and Ibrahim R 2007 *Weld. World* **51** 475
[16] Withers P J and Bhadeshia H K 2001 *Mater. Sci. Technol.* **17** 366
[17] Ziara-Paradowska A M 2007 Investigation of residual stress in welds using neutron and synchrotron diffraction *PhD Thesis* Monash University, Australia
[18] Paradowska A, Finlayson T R, Price J W H, Ibrahim R, Steuwer A and Ripley M 2006 *Physica* B **385–389** 904
[19] Lodini A 2003 Calculation of residual stress from measured strain *Analysis of Residual Stress by Diffraction Using Neutron and Synchrotron Radiation* ed M E Fitzpatrick and A Lodini (London: Taylor and Francis) p 47
[20] Lienert U, Martins R, Grigull S, Pinkerton M, Poulsen H F and Kvick A 2000 *Mater. Res. Soc. Symp. Proc.* **590** 241
[21] Spooner S 2003 Neutron residual stress measurements in welds *Analysis of Residual Stress by Diffraction Using Neutron and Synchrotron Radiation* ed M E Fitzpatrick and A Lodini (London: Taylor and Francis) p 296
[22] Price J W H, Ziara-Paradowska A, Joshi S, Finlayson T R, Semetay C and Nied H 2008 *Int. J. Mech. Sci.* **50** 513